

# Comparison of 3 diffusion models to track the hand motor fibers within the corticospinal tract using functional, anatomical and diffusion MRI

Nicolas Wiest-Daesslé<sup>1,2</sup>, Olivier Commowick<sup>1</sup>, Aymeric Stamm<sup>1</sup>, Patrick Pérez<sup>3</sup>, Christian Barillot<sup>1</sup>, Romuald Seizeur<sup>1,4</sup>, and Sylvain Prima<sup>1</sup>

<sup>1</sup> VISAGES: INSERM U746 - CNRS UMR6074 - INRIA - Univ. of Rennes I, France

<sup>2</sup> Department of Neurology, CHU Rennes, France

<sup>3</sup> Technicolor, Rennes, France

<sup>4</sup> Department of Neurosurgery, CHU Brest, France

**Abstract.** In this paper, we propose to compare three diffusion models to track the portion of the corticospinal tract dedicated to the hand motor function (called hand motor fibers hereafter), using diffusion, functional and anatomical MRI. The clinical diffusion data have few gradient directions and low  $b$ -values. In this context, we show that a newly introduced model, called diffusion directions imaging (DDI) outperforms both the DTI and the ODF models. This new model allows to capture several diffusion directions within a voxel, with only a low number of parameters. Two important results are that i) the DDI model is the only one allowing consistent tracking from the mesencephalon to the most lateral part of the cortical motor hand area, and that ii) the DDI model is the only model able to show that the number of hand motor fibers in the left hemisphere is larger than in the contralateral hemisphere for right-handed subjects; the DDI model, as the other two models, fails to find such a difference for left-handed subjects. To the best of our knowledge, this is the first time such results are reported, at least on clinical data.

## 1 Introduction

Diffusion MRI (dMRI) [11] allows in vivo and non-invasive imaging of tissue structure. It is based on the facts that i) the diffusion of water molecules is constrained by the micro-structure of the tissues (such as, typically, the white matter fibers in the brain), and that ii) MRI can be made sensitive to this diffusion, using specific MR pulse sequences. Diffusion models can then be devised, and their parameters can be estimated for further study and analysis of tissue architecture. The simplest model is that of a Gaussian diffusion function, which amounts to characterise the diffusion with a tensor (*i.e.* a  $3 \times 3$  symmetric definite positive matrix), giving its name to diffusion-tensor imaging (DTI) [2].

Fiber tracking, or tractography, has been developed to “reconstruct” or “dissect” the fiber tracts in vivo, and then infer brain anatomy [18]. Many of the association (*e.g.* uncinate fasciculus, cingulum) and commissural (*e.g.* transverse fibers of the corpus callosum) fiber tracts have been successfully reconstructed

using i) clinical dMRI sequences (with few gradient directions and low  $b$ -values), ii) the simple Gaussian diffusion model and iii) simple deterministic streamline fiber tracking methods [17]. On the contrary, it has proved much more difficult to reconstruct projection fibers, and especially the motor fibers of the corticospinal tract (CST) using such standard protocols. On one side, the anatomy of these fibers between the spinal cord and the internal capsule has been well-studied using DTI [10, 8]. On the other side, the study of these fibers between the internal capsule and the cortex, and in particular of those dedicated to a specific motor function, is much more challenging using DTI, mostly due to the numerous crossings/kissing/merging/diverging fibers in the corona radiata. A particularly difficult fiber bundle to track within the CST is the portion corresponding to the motor hand area, because it is located laterally on the motor cortex [30] (as shown by the homunculus of Penfield & Rasmussen), compared to the leg or the trunk areas for instance. In the following, we call this fiber bundle the HMFs, as “hand motor fibers”.

The HMFs are a crucial fiber bundle to investigate, in the context of normal anatomy, within the more general study of handedness, cerebral dominance, and brain asymmetry [27]. More generally, the development of diffusion models and tractography methods for the CST in general, and the HMFs in particular, which could be used in clinical routine, is key for a better understanding of pathologies of the CST such as, typically, amyotrophic lateral sclerosis [9], Wallerian degeneration of the CST after ischemic stroke [31], motor dysfunctions in infants [14] or in patients with relapsing-remitting multiple sclerosis [13].

New types of image acquisition schemes (*e.g.* HARDI sequences), diffusion models (*e.g.* multiple tensors, ODF, *etc.*) [12] and tractography methods [18–20] have been introduced to account for intricate fiber configurations, but these techniques i) have been reported to often miss entirely the lateral portions of the CST, and thus the HMFs [3] and ii) are not applicable at hand in a clinical setting, mostly due to long acquisition times.

In this paper, we propose to investigate the usefulness of a new diffusion model, termed Diffusion Directions Imaging (DDI), to track the HMFs on clinical data, using a deterministic streamline tractography algorithm. This model allows to capture several diffusion directions within a voxel, with a low number of parameters [26, 4].

The two goals of this paper are: 1) to evaluate the ability of this new diffusion model and of two other standard models (DTI/ODF) to track the left and right HMFs, using a common tractography algorithm, in a clinical setting, *i.e.* with **few diffusion gradients** (typically, less than 15) and **low  $b$ -values** (typically, less than  $1000s/mm^2$ ), and 2) to study whether the number of tracked HMFs in one hemisphere is different from that in the contralateral hemisphere, for right-handed and left-handed subjects. Note that we do not test multi-tensor models, as these have been shown to be unable to provide a unique solution in the context of single-shell (one unique  $b$ -value) acquisitions [24], as is the case here and in most standard clinical protocols.

In Section 2.1, we present the three tested models, and we outline our implementation thereof. In Section 2.2, we describe the common multiple fibers deterministic streamline tractography algorithm we use for these three models. The same algorithm is used to make sure that the subsequently reported results can be interpreted as **differences in models**, rather than differences in dMRI sequences or tractography algorithms. The data are described in Section 2.3, and we perform statistical tests and numerical evaluation in Section 3, before discussing these results, concluding and giving some perspectives in Section 4.

## 2 Material & Methods

### 2.1 Diffusion models

▷ **DTI model**: The **Gaussian model** assumes that the diffusion process can be captured by a tensor (6 parameters), which is proportional to the covariance matrix of the unknown Gaussian pdf. The **tensor**  $T$  is parametrised as  $T = \exp(M)$ , where  $M$  is an unknown  $3 \times 3$  symmetric matrix, and its **estimation** is done using a least-squares (LS) fitting on the raw DWI intensities [7]. The LS criterion is **optimised** numerically using the NEWUOA algorithm [23]. Within a given voxel, the single *putative fiber direction* is considered to be aligned with the direction of the eigenvectors associated to the largest eigenvalue of the tensor. The tractography algorithm uses a **log-Euclidean** interpolation scheme [1].

▷ **ODF model**: The orientation distribution function (**ODF**) describes the orientational structure of the diffusion function [28]. The raw DWI intensities are **modelled** with a modified basis of **spherical harmonics**, whose  $c$  coefficients are **estimated** using a LS fitting including a Laplace-Beltrami regularisation term. The number of unknown coefficients depends on the order  $l$  of the basis:  $c = (l+1)(l+2)/2$ . This LS problem has a closed-form solution, from which the **optimal** ODF (or to be precise, an approximation thereof) can be computed analytically using the Funk-Hecke theorem [5]. Then, ODF sharpening is performed using spherical deconvolution to compute the fiber ODF [6]. Within a given voxel, the putative **fiber directions** are selected as the local maxima of the normalised, sharpened ODF for which the ODF function value is above a user-specified threshold set here to 0.1. These local maxima are computed using NEWUOA (with starting points homogeneously distributed on the unit sphere), and they are sorted according to their ODF function value. The tractography algorithm uses a **trilinear** interpolation scheme [12].

▷ **DDI model**: The diffusion function is **modelled** as a mixture of distributions with a common parametric form [26]. The number of mixture components is that of the number  $m$  of different fiber directions within the voxel. In essence, the pdf of each of these distributions is defined as the convolution of a **von Mises-Fisher** pdf (which models the direction of the fiber) and of a **centered cylindrical Gaussian** pdf (which models the amplitude of the diffusion along the fiber). The covariance matrix of the Gaussian distribution is actually a function

of the two parameters of the von Mises-Fisher distribution: the mean direction  $\mu$  (unit vector) and the concentration parameter  $\kappa$ . A scalar parameter  $\lambda$ , assumed to be identical for all fiber directions, completes the model. Therefore, to allow for  $m$  fibers, the DDI model requires  $3m + 1$  parameters. An anisotropy value  $\xi$ , akin to the fractional anisotropy (FA) (resp. the generalised FA (GFA) [28]) in the DTI (resp. ODF) model, is also defined. The  $3m + 1$  unknown parameters are **estimated** using a LS fitting on the raw DWI intensities, and this **optimisation** is performed using NEWUOA. Within a given voxel, the putative **fiber directions** are a natural output of this model, sorted according to their diffusion function values. Note that, as of now, the number of fibers  $m$  in this model is set to 2, and automated estimation thereof will be a topic of future investigation. The tractography algorithm uses a **trilinear** interpolation scheme.

## 2.2 The common multiple fibers tractography algorithm

Our goal is to track the fibers linking two ROIs. Our deterministic streamline algorithm can be viewed as an extension of the original FACT method [16], adapted to ODF and DDI models, using a *breadth-first*-type search. It must be made clear that for the DTI model, the tractography is led **without** considering multiple directions; we omit this important detail below for the sake of clarity.

Starting from one of the two ROIs, we define  $n$  starting points within each voxel of the ROI. The DTI/ODF/DDI models at these starting points are estimated using the previously described interpolation schemes. For each of these starting points, we compute the two *principal* putative directions (defined using the previously described sorting out procedures), we follow the *first* direction with a step size of  $l$  millimeters and we record the *second* direction for future use, as it can be indicative of crossing/kissing/merging/diverging fibers. We then reestimate the DTI/ODF/DDI models at this new spatial position (using the previously described interpolation schemes), and we compute *all* the putative directions for each model. Among these, we follow the one closest (*i.e.* with minimal angular difference) to the previously estimated first direction. A second direction, having the highest ODF/diffusion function value among the remaining putative fiber directions, is recorded for future use. The tracking of the *main* fiber is achieved when i) the angle between two successively estimated first directions is higher than  $\alpha$ , or when ii) FA/GFA/ $\xi$  is lower than  $\beta$ , or when iii) the fiber reaches the border of a precomputed brain mask [25]. Once this main fiber has been tracked, we perform the same tracking from all the possible crossing/kissing/merging/diverging points that have been recorded along its path. Importantly, for these trackings, the stepping rule and stopping criteria are identical as those for the main fiber, but we do not record any possible mixed fiber configuration along these secondary paths, for which we only follow the first direction at each step. The same tracking is then led on the second ROI, and only the tracts linking the two ROIs are kept for further analysis. In practice, we choose the parameters  $n = 1$ ,  $l = 1$ ,  $\alpha = 60$  degrees and  $\beta = 0.15$ .

### 2.3 Data

The data consist of dMRI, anatomical (aMRI) and functional (fMRI) MRI on 14 right-handed (8 males, 6 females) and 9 left-handed (6 males, 3 females) healthy volunteers. The mean age was 30.3 (21 to 45). Handedness was determined using the Oldfield questionnaire [22]. The aMRI, dMRI and fMRI data were acquired using standard sequences on a Philips Achieva 3T system:

- aMRI: T1-w 3D TFE, 184 sagittal slices of size  $256 \times 256$  ( $1\text{mm} \times 1\text{mm}$ ) and 1mm thickness.
- fMRI: gradient echo EPI using BOLD contrast, 24 contiguous axial slices of size  $128 \times 128$  ( $1.8\text{mm} \times 1.8\text{mm}$ ) and 4mm thickness. The hand motor task consisted in opening and closing the hand, and was implemented in a standard block design. Motion correction, slice-timing and detection of the activation areas for both right and left hands were performed within SPM5.
- dMRI: single shot EPI, 60 contiguous axial slices of size  $128 \times 128$  ( $2\text{mm} \times 2\text{mm}$ ) and 2mm thickness. Diffusion gradients were applied in 15 non-collinear directions with  $b = 800\text{s/mm}^2$ . Each diffusion-weighted MRI was corrected for eddy current-induced geometric distortions [21] and denoised using the Rician non-local means algorithm [29]. Given this low number of directions, the (modified) spherical harmonics basis of order 4 (15 parameters) was used for ODF estimation, while 6 parameters (resp. 7) were to be estimated for the DTI (resp. DDI) model.

For each subject, the aMR and fMR images were rigidly registered to the B0 image of the dMRI sequence [15]. A first ROI was manually delineated by an expert neuroanatomist in an axial slice on the aMRI data through the superior part of the mesencephalum, both on left and right sides. Tractography was then performed between these two anatomical ROIs and the two (left and right) cortical functional ROIs to reconstruct the HMFs using the three above-mentioned diffusion models and the previously described tractography algorithm.

## 3 Results

### 3.1 Connections between the ROIs

Our objective here was to evaluate whether the three diffusion models, coupled with the tractography algorithm, were able to connect fully, partially, or not at all, the anatomical and functional ROIs. First of all, we split each functional ROI into a *medial* and a *lateral* area, the latter corresponding to the extremity of the hand representation on the motor homunculus, *i.e.* the thumb. Then for each model DTI/ODF/DDI, each hemisphere, and each of the 23 subjects, we computed a discrete score of 0, 1 or 2 depending on the *quality/strength* (subjectively based on the number of fibers) of the connection between the anatomical ROI and the medial part of the functional ROI; in a word, we estimated  $3 \times 2 \times 23 = 138$  scores. Similarly, we computed another set of 138 scores for the connection with

the lateral part of the functional ROI. At last, the overall number of fibers composing the reconstructed HMFs, *i.e.* linking the two (anatomical and functional) ROIs, was also computed.

The Pearson  $\chi^2$  test is particularly adequate to handle such qualitative, discrete scores. We performed pairwise Pearson  $\chi^2$  tests with a significance level of 0.05, corrected for multiple comparisons (Bonferroni) to compare DTI vs ODF, ODF vs DDI, and DDI vs DTI for the medial and lateral areas. To compare the overall number of fibers, we first showed that the data were not Gaussian-distributed using the Jarque-Bera test, and then we performed pairwise sign tests (which allows to test for differences in medians) with a significance level of 0.05, corrected for multiple comparisons (Bonferroni).

The  $p$ -values are reported in Tab. 1, left, and mainly show that i) the ODF model was able to track more medial fibers than the DTI model, but as many lateral fibers, and that ii) the DDI model did not track more medial fibers than the ODF model, but did track more lateral fibers, at the 0.05 significance level. These two results are confirmed by the sign test on the overall number of fibers.

### 3.2 Asymmetry of the hand motor fibers

Our objective here was to evaluate whether the three diffusion models, coupled with the tractography algorithm, were able to show significant differences (in terms of number of fibers) between the left and right reconstructed HMFs, in right-handed (14) and left-handed (9) subjects. We pooled males and females for increased statistical power. After showing that the data were not Gaussian-distributed using the Jarque-Bera test, we performed pairwise sign tests with a significance level of 0.05, corrected for multiple comparisons (Bonferroni).

The  $p$ -values are reported in Tab. 1, right, and mainly show that i) none of the models is able to show differences in left-handed subjects, but that ii) the DDI model is the only model allowing to show that the bundle of HMFs is *larger* (in terms of number of fibers) in the left hemisphere than in the right for right-handed subjects.

	Medial	Lateral	# Fibers		RH	LH
DTI vs ODF	$2.6 \times 10^{-9}$	$3.4 \times 10^{-1}$	$3.3 \times 10^{-7}$	DTI	0.0923	1
ODF vs DDI	$3.7 \times 10^{-2}$	$7.6 \times 10^{-12}$	$3.1 \times 10^{-7}$	ODF	0.5811	0.1797
DDI vs DTI	$1.3 \times 10^{-14}$	$5.5 \times 10^{-14}$	$2.8 \times 10^{-14}$	DDI	0.0189	0.5078

**Table 1.  $p$ -values of the statistical tests.** Left table: “Is there a significant difference (level=0.05) between the 3 models in recovering tracts reaching the medial and lateral areas of the functional ROI, in each hemisphere, for the 23 subjects? And in the overall number of tracked fibers?”. Right table: “Are the 3 models able to show significant differences (level=0.05), in terms of number of fibers, between the left and right tracked HMFs, for the 14 right-handed (RH) and the 9 left-handed (LH) subjects?”.

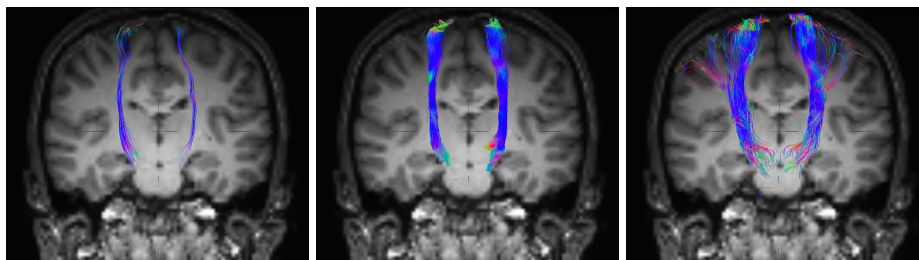


**Fig. 1. Tractography of the HMFs in the left and right hemispheres.** From left to right: DTI, ODF and DDI. Note that we use the neurological convention, *i.e.* the left (resp. right) hemisphere is displayed on the left (resp. right). The DDI model is the only one able to consistently reach the lateral area within the functional ROI.

#### 4 Discussion, Conclusion & Perspectives

In this paper, we showed that i) the DDI model outperforms both the DTI and the ODF models to track the HMFs (see Fig. 1), and, maybe more importantly, that ii) the DDI model is the only model able to show that the number of HMFs in the left hemisphere is larger than in the contralateral hemisphere for right-handed subjects, which seems to fit the intuitive idea that the hand motor fibers in the hemisphere contralateral to the dominant hand *should* be somewhat *more developed* than those in the other hemisphere. Interestingly, the DDI model, as the other two models, failed to find such a difference for left-handed subjects, which may suggest that left-handedness is not simply a *mirrored* right-handedness. This is already known from *e.g.* the notoriously differing patterns of hemispheric dominance for language between left and right-handed subjects, but to our knowledge, this is the first time such results are reported on white matter fibers, at least on clinical data. These results must now be further investigated in light of the huge literature on brain asymmetry and cerebral dominance [27]. In particular, recruiting more males/females and right/left-handed subjects for increased statistical power and population-specific analysis would be necessary to confirm these first results, of potentially important anatomical significance.

As expected, the DTI model performs very poorly when tracking the HMFs. Importantly, we stress here that we do *not* state that the DDI model outperforms the ODF model in general, but only in this particular experimental setting. Low angular resolution of the order-4 ODF model can explain why it is outperformed here. It would be of high interest to try to replicate our experiments on HARDI data using higher-order ODF models and improved (*e.g.* probabilistic) tractography methods, to further support our first findings.

#### References

1. Arsigny, V., Fillard, P. et al.: Log-Euclidean metrics for fast and simple calculus on diffusion tensors. *Magn Reson Med* 56(2), 411–421 (2006)

2. Basser, P., Jones, D.: Diffusion-tensor MRI: theory, experimental design and data analysis - a technical review. *NMR in Biomedicine* 15(7–8), 456–467 (2002)
3. Behrens, T.E.J., Berg, H.J. et al.: Probabilistic diffusion tractography with multiple fibre orientations: What can we gain? *Neuroimage* 34(1), 144–155 (2007)
4. Commowick, O., Stamm, A. et al.: Multifiber deterministic streamline tractography of the corticospinal tract based on a new diffusion model. *DTI Tractography for Neurosurgical Planning: A Grand Challenge – MICCAI Workshop* (2011)
5. Descoteaux, M., Angelino, E. et al.: Regularized, fast, and robust analytical Q-ball imaging. *Magn Reson Med* 58(3), 497–510 (2007)
6. Descoteaux, M., Deriche, R. et al.: Deterministic and probabilistic tractography based on complex fibre orientation distributions. *IEEE Trans Med Imaging* 28(2), 269–286 (2009)
7. Fillard, P., Pennec, X. et al.: Clinical DT-MRI estimation, smoothing, and fiber tracking with log-Euclidean metrics. *IEEE Trans Med Imaging* 26(11), 1472–1482 (2007)
8. Hong, J.H., Son, S.M., Jang, S.H.: Somatotopic location of corticospinal tract at pons in human brain: a diffusion tensor tractography study. *Neuroimage* 51(3), 952–955 (2010)
9. Iwata, N.K., Aoki, S. et al.: Evaluation of corticospinal tracts in ALS with diffusion tensor MRI and brainstem stimulation. *Neurology* 70(7), 528–532 (2008)
10. Kim, Y.H., Kim, D.S. et al.: Corticospinal tract location in internal capsule of human brain: diffusion tensor tractography and functional MRI study. *Neuroreport* 19(8), 817–820 (2008)
11. Le Bihan, D.: Looking into the functional architecture of the brain with diffusion MRI. *Nature Reviews Neuroscience* 4(6), 469–480 (2003)
12. Lenglet, C., Campbell, J.S.W. et al.: Mathematical methods for diffusion MRI processing. *Neuroimage* 45(1 Suppl), S111–S122 (2009)
13. Lin, F., Yu, C. et al.: Diffusion tensor tractography-based group mapping of the pyramidal tract in relapsing-remitting multiple sclerosis patients. *Am J Neuroradiol* 28(2), 278–282 (2007)
14. Ludeman, N.A., Berman, J.I. et al.: Diffusion tensor imaging of the pyramidal tracts in infants with motor dysfunction. *Neurology* 71(21), 1676–1682 (2008)
15. Maes, F., Collignon, A. et al.: Multimodality image registration by maximization of mutual information. *IEEE Transactions on Medical Imaging* 16(2), 187–198 (1997)
16. Mori, S., Crain, B.J. et al.: Three-dimensional tracking of axonal projections in the brain by magnetic resonance imaging. *Ann Neurol* 45(2), 265–269 (1999)
17. Mori, S., Wakana, S. et al.: *MRI Atlas of Human White Matter*. Elsevier (2005)
18. Mori, S., van Zijl, P.: Fiber tracking: principles and strategies - a technical review. *NMR in Biomedicine* 15(7–8), 468–480 (2002)
19. Mukherjee, P., Berman, J.I. et al.: Diffusion tensor MR imaging and fiber tractography: theoretic underpinnings. *Am J Neuroradiol* 29(4), 632–641 (2008)
20. Mukherjee, P., Chung, S.W. et al.: Diffusion tensor MR imaging and fiber tractography: technical considerations. *Am J Neuroradiol* 29(5), 843–852 (2008)
21. Netsch, T., van Muiswinkel, A.: Quantitative evaluation of image-based distortion correction in diffusion tensor imaging. *IEEE Trans Med Imaging* 23(7), 789–798 (2004)
22. Oldfield, R.C.: The assessment and analysis of handedness: the Edinburgh inventory. *Neuropsychologia* 9(1), 97–113 (1971)
23. Powell, M.: *The NEWUOA software for unconstrained optimization without derivatives*. Springer (2004)

24. Scherrer, B., Warfield, S.K.: Why multiple b-values are required for multi-tensor models. Evaluation with a constrained log-Euclidean model. ISBI, 1389–1392 (2010)
25. Smith, S.M.: Fast robust automated brain extraction. HBM 17(3), 143–155 (2002)
26. Stamm, A., Pérez, P., Barillot, C.: Diffusion Directions Imaging (DDI). INRIA Technical Report (2011)
27. Toga, A., Thompson, P.: Mapping brain asymmetry. Nature Reviews Neuroscience 4(1), 37–48 (2003)
28. Tuch, D.: Q-ball imaging. Magnetic Resonance in Medicine 52(6), 1358–1372 (2004)
29. Wiest-Daesslé, N., Prima, S. et al.: Rician noise removal by non-local means filtering for low signal-to-noise ratio MRI: applications to DT-MRI. MICCAI (Pt 2), 171–179 (2008)
30. Yousry, T.A., Schmid, U.D. et al.: Localization of the motor hand area to a knob on the precentral gyrus. A new landmark. Brain 120 (Pt 1), 141–157 (1997)
31. Yu, C., Zhu, C. et al.: A longitudinal diffusion tensor imaging study on Wallerian degeneration of corticospinal tract after motor pathway stroke. Neuroimage 47(2), 451–458 (2009)